Fabrication of Silicon Nanowire Arrays by Near-Field Laser Ablation and Metal-Assisted Chemical Etching

Daniel Brodoceanu, Hashim Z. Alhmoud, Roey Elnathan, Bahman Delalat, Nicolas H. Voelcker, and Tobias Kraus

Nanotechnology 27(7)

Keywords:
laser nanopatterning, near-field ablation, silicon nanowire array, porous silicon, metal-assisted chemical etching

Fabrication of silicon nanowire arrays by near-field laser ablation and metal-assisted chemical etching

D Brodoceanu[1], H Z Alhmoud[2], R Elnathan[2], B Delalat[2], N H Voelcker[2] and T Kraus[1]

[1] INM-Leibniz Institute for New Materials, Saarbrücken 66123, Campus D2 2, Germany,
[2] Mawson Institute, University of South Australia, Adelaide, SA 5001, Australia

E-mails: daniel.brodoceanu@leibniz-inm.de, tobias.kraus@leibniz-inm.de

Abstract

We present an elegant route for the fabrication of ordered arrays of vertically-aligned silicon nanowires with tunable geometry at controlled locations on a silicon wafer. A monolayer of transparent microspheres convectively assembled onto a gold-coated silicon wafer acts as microlens array. Irradiation with a single nanosecond laser pulse removes the gold beneath each focusing microsphere, leaving behind a hexagonal pattern of holes in the gold layer. Owing to the near-field effects, the diameter of the holes can be at least 5 times smaller than the laser wavelength. The patterned gold layer is used as catalyst in a metal-assisted chemical etching to produce an array of vertically-aligned silicon nanowires. This approach combines the advantages of direct laser writing with the benefits of parallel laser processing, yielding nanowire arrays with controlled geometry at predefined locations on the silicon surface. The fabricated VA-SiNW arrays can effectively transfect human cells with a plasmid encoding for green fluorescent protein.

Keywords: laser nanopatterning, near-field ablation, silicon nanowire array, porous silicon, metal-assisted chemical etching

1. Introduction

Arrays of vertically aligned silicon nanowires (VA-SiNW) have been proposed as a base material for technology applications, from sensors [1] and solar cells [2, 3] to Li-ion batteries [4] and substrates for surface-assisted laser desorption/ionization mass spectrometry (SALDI-MS) [5]. They are also used for life science applications such as cell transfection, [6, 7] templates for studying cell motility, [8, 9] and drug delivery devices [10]. Existing fabrication methods for ordered arrays of VA-SiNW rely on patterning techniques such as photolithography [11], interference lithography [12, 13], nanoimprint [14] or colloidal lithography [15, 16] in combination with subsequent processes such as vapor–liquid–solid growth (VLS) [17], deep reactive ion etching (DRIE) [18] or metal-assisted chemical etching (MACE) [19, 20]. Colloidal lithography, also known as nanosphere lithography, combined with MACE is a very popular strategy employed for the fabrication of VA-SiNW. Typically, a self-assembled monolayer of polymer microspheres is exposed to reactive ion etching (RIE) in order to reduce the diameter of the microspheres, yielding a non-close packed (ncp) array. The ncp array is then used as a mask during the deposition of a noble metal layer. The resulting patterned metal layer is used as catalyst in a MACE process that yields arrays of VA-SiNW [19-22].

Here we present a different particle-based strategy that allows fabrication of multiple VA-SiNW arrays with tunable wire diameter at desired locations on a same silicon wafer. In contrast to the widely reported nanosphere lithography where particles are used as masks for subsequent metal deposition, our strategy exploits self-assembled particles as microlens arrays for the near-field patterning of noble metal layers. A self-assembled monolayer of transparent microspheres can act as a microlens array able to focus a laser beam onto the surface of an underlying substrate, an approach that has been used for the near-field patterning of various substrates, but rarely employed for the patterning of metal thin films [23-26]. We combine the near-field nanopatterning of gold thin film with MACE to create ordered arrays of VA-SiNW with tunable geometries, a combination that has not been accomplished before to the best of our knowledge. A close-packed monolayer of polymer microsphere is assembled on a gold-coated silicon wafer and irradiated by single ns-laser pulse to remove the gold layer underneath, yielding a hexagonal pattern of uniform circular holes that retain the order of the monolayer. The patterned gold layer is an excellent catalyst for the MACE process. The etch yields VA-

SiNW arrays at precise locations defined by the *x*-*y* coordinates of the laser spot on the sample. This enables "direct writing" of SiNW arrays, for example to integrate VA-SiNW into lab-on-chip applications.

2. Experimental details

Colloidal suspensions of monodispersed polystyrene (PS) microspheres with mean diameters of 1 μm and 500 nm were acquired from BangsLabs, (USA). Silicon substrates (<100> p-type, resistivity 5–30 mOhm·cm, Si-Mat) were cleaned in an ultrasonic bath using isopropanol (Sigma-Aldrich), rinsed with deionized water (Millipore) and dried under a nitrogen stream. Gold thin films with thickness in the range of 20-30 nm were deposited on silicon wafer (coated by native oxide) using a standard DC magnetron sputter-deposition system (Autofine Coater, JEOL). The gold-coated substrates were treated in oxygen plasma for 30 s at 0.3 mbar (low-pressure reactor PICO, RF source at 13.56 MHz, Diener electronic, Ebhausen, Germany) at 50 W RF power to render the metal surface hydrophilic for the PS microsphere monolayer assembly. Close-packed PS microsphere monolayers were then convectively assembled on the gold coated silicon surface with area of ~2 cm^2 (Figure S1, Supplementary Information) using a setup described in a previous report [27]. After monolayer assembly, some samples were treated with RF oxygen plasma (0.3 mbar, P = 50 W) for 12 min to reduce the diameter of the PS microspheres from 1 μm to 750 nm, resulting in a non-close-packed array [28].

Laser irradiation was performed using a Q-switched Nd:YAG laser system (Quanta-Ray Pro 290, Spectra Physics, pulse duration 10 ns) operating at the third harmonic (λ = 355 nm). The gold coated silicon substrate with the particle-based microlens array on top was mounted on a *x*-*y* translation stage. A red laser diode (P < 1 mW) was used for guiding the ns-laser at precise locations across the sample. The spot size of the ns-laser was in the range of 0.2-2 mm. The laser energy was measured using a laser power meter (Ophir), considering the losses (~ 8 %) introduced by the optical components used in the experiment (i.e. focusing lens, deflecting mirror). The laser fluence was determined by dividing the measured laser energy to the laser spot produced on the sample surface. The PS refractive index used for the Mie calculations was n = 1.6 at λ = 355 nm. After irradiation, the remaining PS microspheres were dissolved in toluene.

The MACE process was carried out at room temperature by immersing the silicon piece holding the perforated gold layer for 1 - 13 min in a Teflon beaker containing an etching mixture of deionized water, HF, and H_2O_2 with concentrations 4.6 M and 0.44 M, respectively. After etching, the samples were rinsed in deionized water and dried under nitrogen stream.

For the cell transfection experiment, Human embryonic kidney (HEK293, ATCC CRL-1573) cells were grown and maintained at 37 °C with 5% CO_2 in DMEM supplemented with 10 % fetal bovine serum (FBS, Sigma-Aldrich), 2 mM L-glutamine, 100 U/mL penicillin, and 100 g/mL streptomycin (Invitrogen), for 2–3 d until they were 70–80 % confluent. The adherent cells were detached and harvested by using 0.05% trypsin/EDTA solution treatment. After trypsinization, the cells were seeded at a density of 1×10^5 cells/mL in complete DMEM medium. The VA-SiNW substrates were used for transfection of high-expression green fluorescent protein vector (gWiz™ GFP, Aldevron) into HEK293 cells. To functionalize the VA-SiNW substrates with the plasmid, the substrates were first placed in a 24-well sterile format, then sterilized in 70% ethanol and allowed to dry at room temperature for 2 h. The VA-SiNW substrates were subsequently coated with poly-D-lysine at concentration of 167 μg/L and incubated at 4 °C overnight, followed by washing step with PBS (phosphate buffered saline). The gWiz™ GFP was diluted to 20 μg/mL in PBS and 100 μL of this solution was added per well containing the substrates which were then incubated overnight at 4 °C. Unbound plasmid was washed off with PBS. The HEK293 cells were seeded at a density of 5×10^5 cells/mL in Opti-MEM medium (Life Technology) onto the plasmid coated VA-SiNW substrates. Afterwards, the samples were incubated for 4-6 h at 37 °C in a humidified atmosphere with 5 % CO_2. The Opti-MEM medium was subsequently replaced with a complete medium containing DMEM, FBS 10 % and incubated at 37 °C for 72 h. To assess the delivery of eGFP reporter gene into HEK293 cells, fluorescence images of the transfected cells were recorded under inverted fluorescence microscope (Nikon TiS). WinTube software (Wimasis GmbH, Munich, Germany) was used for counting the number of total cells and GFP positive cells that allowed calculating the transfection efficiency.

3. Results and discussion

The main processing steps are displayed in Figure 1. Fabrication starts with the convective assembly of submicron polystyrene (PS) microspheres on a gold-coated silicon substrate of about 2 cm^2 (Figure 1d). A ns-laser pulse generated by a frequency-tripled Nd:YAG laser (λ = 355 nm, τ = 10 ns) is focused into millimeter-sized spot on the sample that moves on a *x-y* translation stage. Figure S2 (Supplementary information) shows separated spots on the surface of the microsphere monolayer after single-pulse laser irradiations. The PS spheres act as microlenses for a single laser pulse that generates an ordered array of well-defined holes into the gold layer (Figure 1e). The bright rims surrounding the holes form by near-field ablation followed by dewetting of gold on the silicon surface. The rims are smooth and compact that make these holes particularly suitable as catalyst for MACE to yield arrays of VA-SiNW (Figure 1f).

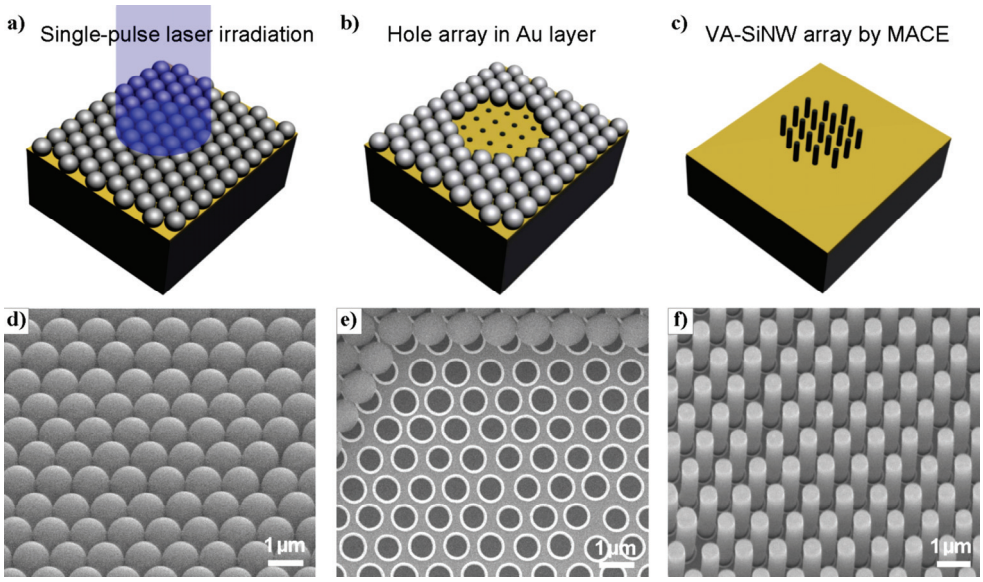

Figure 1. Process flow for the fabrication of VA-SiNW arrays. (a-c) Schematic illustration of the main steps. (d) Scanning Electron Microscopy (SEM) image of a PS microlens array convectively assembled on the gold-coated silicon wafer. (e) Top-view SEM image of a hole array in a gold layer produced by irradiating the microlenses with a single laser pulse (λ = 355 nm, τ = 10 ns, $\phi \approx$ 30 mJ/cm^2). (f) Tilted SEM image of the array of VA-SiNW after 13 min MACE etching.

Mie-theory calculations predict the optical field enhancement beneath a focusing sphere, depending on its diameter, refractive index and laser wavelength [23, 29]. Our calculations show that PS microspheres (n = 1.6) provide field enhancements between S_z^* = 36 (for 1 µm PS) and S_z^* = 12 (for 500 nm PS) at a laser

wavelength of λ = 355 nm, in the *xy*-plane directly below microspheres (Figure 2). Considering the measured laser fluence incident on the PS microlens arrays in the range of 11-55 mJ/cm^2, the fluence on the gold layer below a focusing microsphere with a diameter of 1 µm is estimated in the range of 400 mJ/cm^2 to 2J/cm^2 for a field enhancement of S_z^* = 36 (Figure 2a).

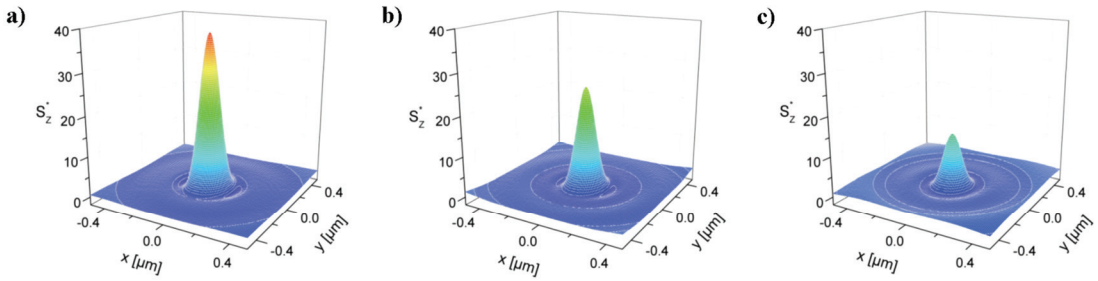

Figure 2. Calculated *z*-component of the Poynting intensity distribution in the *x*-*y* plane right under laser-irradiated PS microspheres of different diameters *D*. (a) *D* = 1 µm (b) *D* = 750 nm and (c) *D* = 500 nm.

Arrays of holes with diameters depending on laser fluence and microspheres size were fabricated in gold-coated silicon wafers. Figure 3 displays typical arrays in a 30 nm thick gold layer formed underneath PS microspheres with a diameter of 1 µm. Figure S3 (Supplementary Information) shows hole arrays achieved under extreme laser fluences. With 500 nm PS spheres assembled on a gold layer of same thickness (30 nm), the holes were less homogenous or incompletely formed (Figure S4, Supplementary Information) that we attribute to the lower field enhancement shown in Figure 2c and the smaller diameter of the near-filed spot that becomes comparable with the gold layer thickness. In addition, the gold ablation threshold is expected to increase with thickness [30]. Decreasing the thickness of gold layer from 30 nm to 20 nm resulted in uniform holes with smaller size than those achieved with 1 µm PS (Figure 4 b-c). Thus, 500 nm PS microspheres irradiated at low fluences (15-30 mJ/cm^2) formed nanoholes with diameters less than 70 nm in the 20 nm gold layer, which is below 1/5 of the laser wavelength. The main contribution to the formation of sub-wavelength holes is attributed to the optical near-field effects [31-33]. In addition, we believe that the controlled dewetting of gold thin film on the silicon surface essentially contributes to the definition of the submicron holes with round shape and homogenous border as seen in Figure 3.

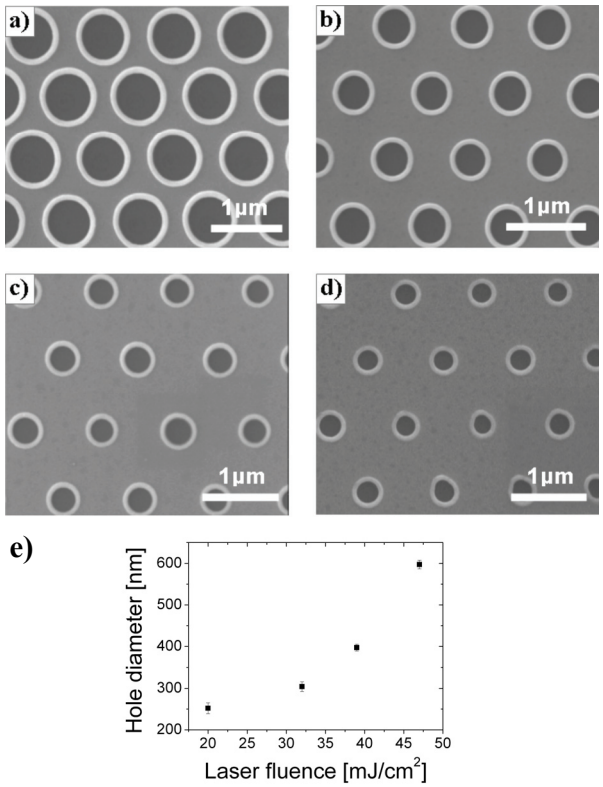

Figure 3. Scanning electron micrographs of holes achieved in 30 nm thick gold layer irradiated through the microlens array with single laser pulse (λ = 355 nm, τ = 10 ns) at different laser fluences ϕ: (a) $\phi \approx$ 33 mJ/cm^2, (b) $\phi \approx$ 27 mJ/cm^2, (c) $\phi \approx$ 22 mJ/cm^2, (d) $\phi \approx$ 14 mJ/cm^2. (e) Relation between hole diameter and fluence. Error bars represent standard deviation.

The focused laser beam reaches the underlying gold layer where the laser energy is absorbed and converted into heat. Material properties, geometry and laser pulse duration τ_l determine a characteristic heat diffusion length l_T in the metal layer and ultimately set the resolution of the generated features:

$$l_T \approx \sqrt{D\,\tau_l}$$

where D is the thermal diffusivity of the gold layer considered and τ_l is the laser pulse duration [34]. The thermal diffusivity of gold thin films with thickness below 30 nm was reported to be about an order of magnitude lower than in bulk [35]. If we consider the thermal diffusivity of gold layer with thickness of 20 nm to be about $8 \cdot 10^{-6}$ m^2/s and the laser pulse duration of τ_l = 10 ns (Q-switched Nd:YAG), the heat diffusion length is estimated at 280 nm. In our experiments, however, the smallest holes were below 70 nm in diameter when using PS microspheres with diameter of 500 nm (Figure 4).

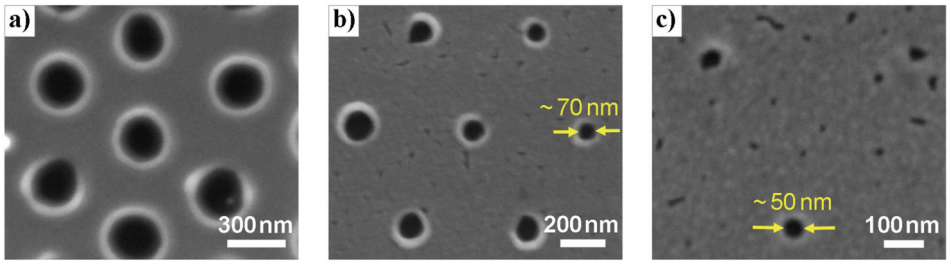

Figure 4. Typical arrays of holes generated in 20 nm thick gold layer using a microlens array of PS microspheres with diameter of 500 nm irradiated by single-pulse laser at different laser fluence (a) $\phi \approx 43$ mJ/cm^2, $D = 270 \pm 20$ nm (b) $\phi \approx 28$ mJ/cm^2, $D = 87 \pm 20$ nm (c) Smallest holes ($D \approx 50$ nm) observed at $\phi \approx 16$ mJ/cm^2.

The laser energy couples into the metal layer within a near-field spot with size of few tens of nanometres that can locally induce melting or ablation, depending on laser fluence. As the optical penetration depth of the gold at $\lambda = 355$ nm is about 16 nm, most of the laser radiation is converted into heat within the metal layer [36]. The laser-induced heat propagates at higher rate within the gold layer than into silicon substrate, because of the increased thermal diffusivity of the gold. In addition, the presence of the native silicon oxide may considerably limit the heat transfer between gold film and silicon surface [37]. As a consequence, an in-plane temperature gradient develops in the metal film around the near-field spot where the temperature reaches its maximum. It is conceivable that the nanoholes form close to ablation threshold, due to surface instability induced by rapid thermal expansion, followed by gold dewetting on silicon surface [38, 39]. The gold eventually cools down, resulting in the circular holes with homogenous rims that we observe. This would also explain the behaviour of the PS microspheres during laser irradiation. Laser ablation implies temperatures of a few thousands K [34]. One would expect removal of the focusing microspheres under such conditions, as previously reported [23, 40]. We did observe removal of PS microspheres (D = 1μm) at the center of irradiated spot with laser fluences exceeding 70 mJ/cm^2. The SEM image in Figure S2a, (Supplementary Information) reveals complete ablation of the gold layer in the central region of the spots, because of Gaussian intensity profile of the laser beam, while hole arrays formed at periphery at a lower fluence. Typically, within the fluence range required for the formation of holes in gold layer, the PS microspheres remained on top of the generated holes, as shown in Figure 1e, suggesting dewetting of gold induced by the near-field irradiation close to ablation threshold. That is also consistent with the incomplete

formation of holes in 30 nm thick gold layer shown in Figure S4 (Supplementary Information) and with the irregular profiles of the holes produced on cracked gold layer (Figure S5, Supplementary Information). No ablation craters were observed on the silicon surface exposed at the center of the generated holes in gold, even at high fluence range (Figure S3b, Supplementary Information). Both size and shape of the hole array in gold layer depend on the laser beam profile during monolayer irradiation. Round spots of hole arrays were generated on the sample with the laser beam focused using a spherical lens (f = 5 cm). By using a cylindrical lens (f = 5 cm), hole arrays with length up to 5 mm and width below 20 μm could be achieved (Figure S2b, Supplementary Information). The method can be scaled up to uniformly process large sample areas by expanding the laser beam diameter and homogenizing the beam intensity profile. For example, the energy per pulse needed to fabricate one cm^2 of hole arrays similar to the one shown in Figure 3c is 22 mJ. Considering that a common Q-switched YAG:Nd laser can routinely deliver at least 300 mJ/pulse at the 3^{rd} harmonic (λ= 355 nm), the size of the hole array generated with single pulse can be of the order of more than 10 cm^2. To fabricate such large arrays with identical hole diameter, however, the laser beam should have uniform intensity profile.

The diameter of the microlenses can be decreased using RF oxygen plasma [28], allowing to decouple the pitch of the array from the desired hole size. Figure S6 (Supplementary Information) shows an ordered array of non-close-packed array of PS microspheres produced by isotropic etching in RF oxygen plasma that reduced the PS microspheres' diameter from 1 μm to about 750 nm. The etched microspheres produced smaller holes after single-pulse laser irradiation. We conclude that etching in RF oxygen plasma does not critically affect the focusing properties of PS microspheres.

The perforated metal layers were employed as a catalyst for MACE etching to fabricate smooth VA-SiNW with controlled diameter, length, cross-section profile and spacing. Figure 5 displays arrays of VA-SiNW from holes generated at two laser fluences using PS microspheres with diameter of 1 μm. Sparse arrays of VA-SiNW that are challenging to achieve with the common route based on colloidal lithography and MACE are readily obtained here (Figure 5d). The distance between nanowires is solely dictated by the original microsphere size.

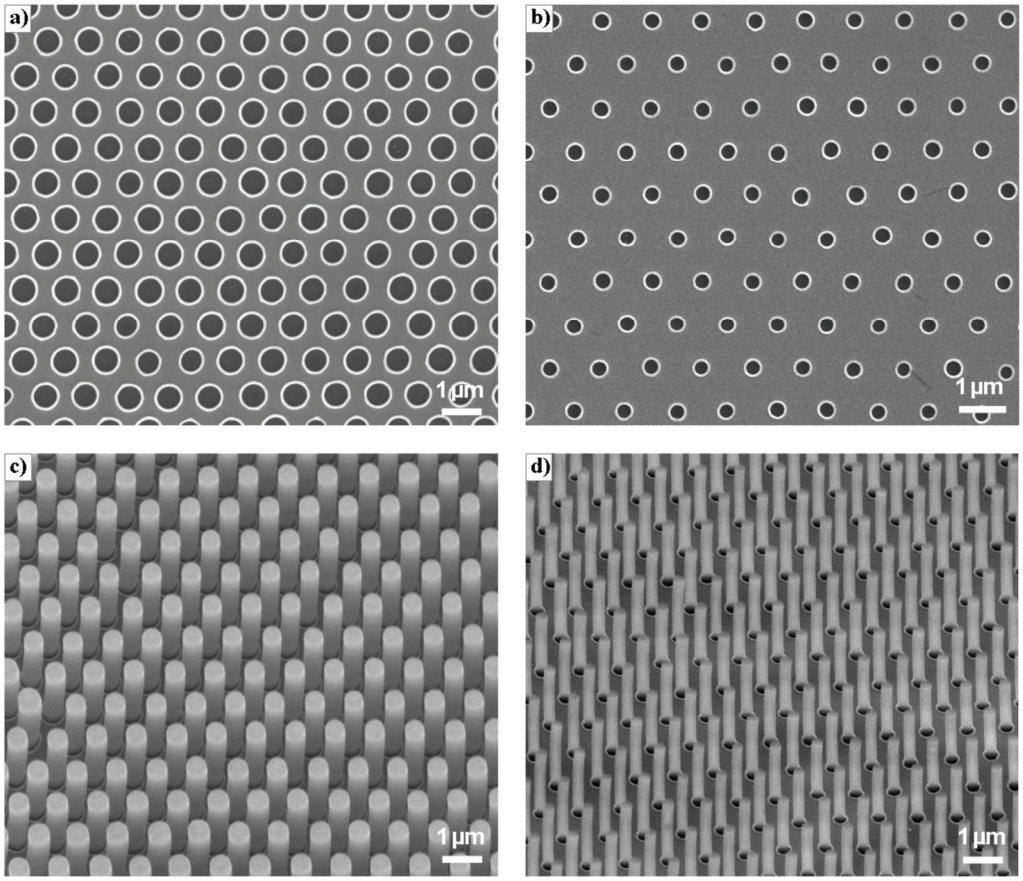

Figure 5. Ordered arrays of smooth VA-SiNW formed by MACE etching using laser-drilled gold films as catalysts generated using PS microspheres with diameter of 1 µm. (a) Array of holes with diameter of 515 ± 23 nm generated in 30 nm gold layer by single-pulse laser irradiation (λ = 355 nm, $\phi \approx$ 30 mJ/cm^2) through PS microlenses. (b) Smaller holes (245 ± 16 nm) generated at a fluence of $\phi \approx$ 16 mJ/cm^2 (c) Tilted SEM micrograph of VA-SiNW emerging from the hole array in gold shown in (a) after 13 min MACE. (d) Sparse array of VA-SiNW resulted from holes displayed in (b) after 13 min MACE.

Typical array of holes and the resulting VA-SiNW obtained with PS microspheres with diameter of 500 nm are shown in Figure 6.

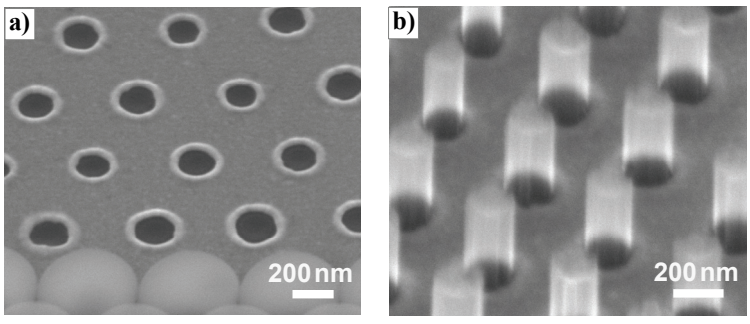

Figure 6. Laser patterned gold layer and the resulting VA-SiNW obtained using PS microspheres with diameter of 500 nm as microlenses**.** (a) Array of holes with diameters ranging from 170 nm to 200 nm generated in a 20 nm gold layer following single-pulse laser irradiation (λ = 355 nm, $\phi \approx$ 40 mJ/cm^2) through the PS monolayer. (b) Array of VA-SiNW with same diameter as the holes counterparts seen in (a) and length of about 360 nm resulted after 2 min MACE etching.

The VA-SiNW diameter can be tuned by controlling the size of the holes generated in the gold layer at different laser fluences. For example, Figure 7 displays VA-SiNW with diameter ranging from ≈ 280 nm to ≈ 720 nm achieved using single-pulse laser shots with fluence in the range of 14 – 35 mJ/cm^2.

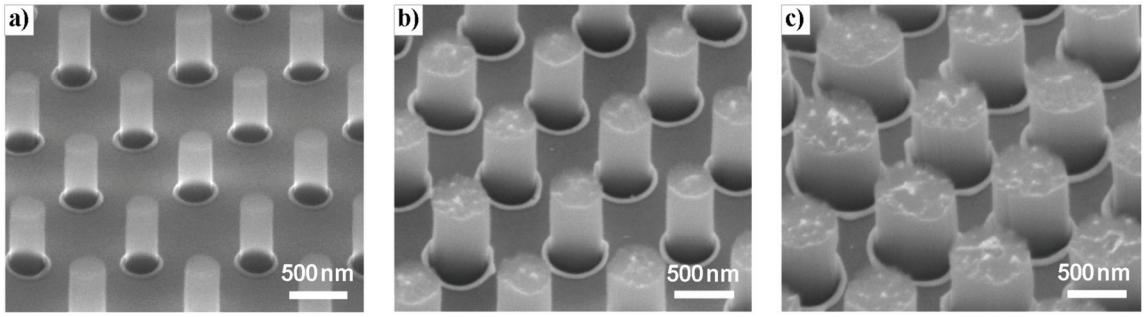

Figure 7. Tuning the VA-SiNW diameter using the hole arrays in gold layers generated at different laser fluences: (a) $\phi \approx$ 14 mJ/cm^2, (b) $\phi \approx$ 27 mJ/cm^2, (c) $\phi \approx$ 35 mJ/cm^2. The MACE etching time was 3 min.

As expected, the nanowire length is set by MACE etching time. The etching rate was estimated to 180 nm/min. Figure 8 shows typical arrays of VA-SiNW with different aspect ratios achieved using arrays of holes of same diameter following MACE at various etching times.

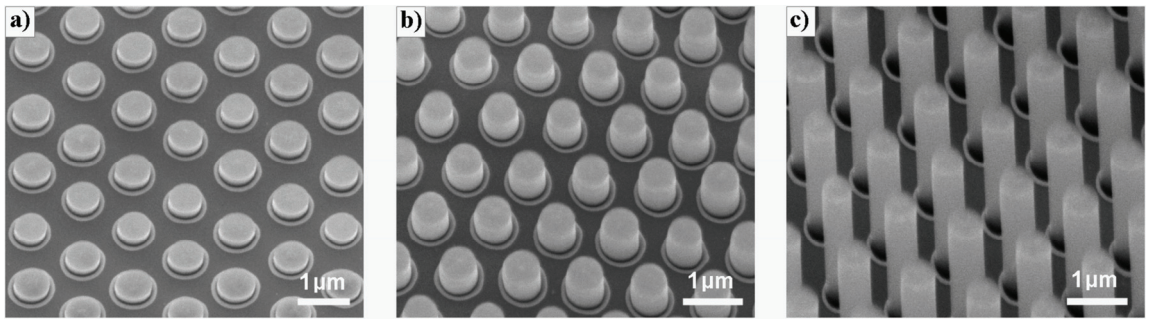

Figure 8. Arrays of VA-SiNW with different aspect ratios set by MACE etching time: (a) 1 min, $\Gamma \approx 0.25$ (b) 5 min, $\Gamma \approx 1.4$ and (c) 13 min, $\Gamma \approx 4$. The etching rate was estimated at 180 nm/min.

We were also able to change the cross-section profile of the SiNW, using a patterning approach previously reported [41]. By irradiating the PS monolayer at two different angles of incidence, arrays of holes with asymmetric shapes were generated in gold thin films that were subsequently transferred into the underlying silicon using MACE (Figure 9). This technique enables control of the cross-section profile.

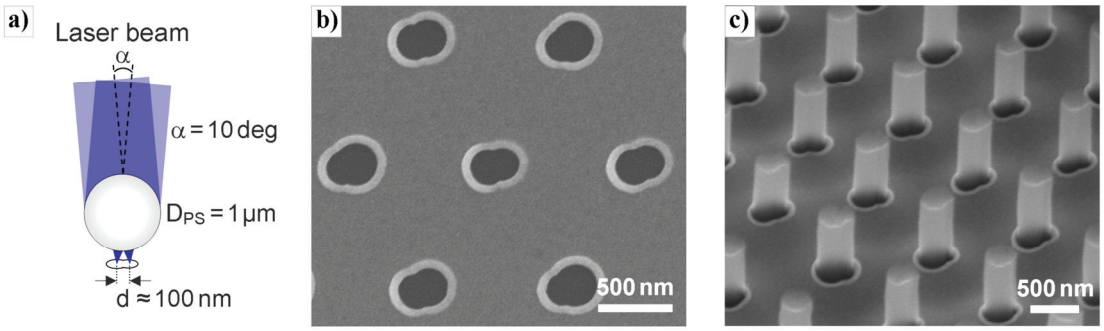

Figure 9. Fabrication of VA-SiNW with non-circular cross-section profile. (a) Schematic illustration showing the shift in lateral position of the laser focal spot under the microsphere irradiated at two different angles of incidence. (b) SEM micrograph of perforated gold layer with asymmetric shaped holes. (c) Resulted array of VA-SiNW after 4 min MACE using as catalyst the hole array in gold layer shown in (b).

Our strategy for the fabrication of VA-SiNW arrays is substantially different from the widely reported route based on colloidal lithography combined with MACE. Whereas in colloidal lithography the particles are used as masks, we employ the particles as microlenses. This enables tuning of the SiNW diameter and SiNW cross-sectional profile. Furthermore, multiple VA-SiNW arrays with controlled dimensions depending on laser spot geometry can be fabricated at desired positions on the same sample. Parallel fabrication of ordered arrays of VA-SiNW with diameter gradient can be readily achieved using laser beams with Gaussian profile.

One of the important applications of VA-SiNW that requires precisely defined geometry is cell transfection, where genes are delivered inside cells by penetrating the membrane without disrupting the cell function [6]. Cell transfection has been demonstrated previously using nanowires from VLS-based, MOVPE, and RIE growth processes [42]. Human embryonic kidney 293 (HEK293T) cells are often used to study cell function and behavior and are an important model cell system for transfection studies [43]. We tested whether our laser-fabricated sparse array of VA-SiNW are suitable as an in vitro platform for transfecting HEK293T cells using eGFP as reporter gene. The VA-SiNW arrays were functionalized with poly-D-lysine (PDL) to allow plasmid sorption and to confer better cell adhesion. The fluorescence image in Figure S7 (Supplementary Information) indicates successful delivery of eGFP into HEK293 cells, with a transfection efficiency exceeding 54 %. This result achieved with a VA-SiNW array without optimization confirms our expectation concerning the feasibility of this fabrication route for engineering of efficient cell transfection platforms. Further work is in progress to fabricate arrays of VA-SiNW with optimum geometry for maximizing the transfection efficiency.

Conclusions

Ordered arrays of VA-SiNW were fabricated by single-pulse laser irradiation of self-assembled polymer microspheres employed as microlens array to drill holes in a gold layer that acted as catalyst in a MACE process. We showed that ns-laser processing in the near-field can form holes with diameter at least 5 times smaller than the laser wavelength and discussed their formation mechanism. The holes were compact and homogenous, with diameters readily tuned within large limits by simply adjusting the laser fluence. We were able to tailor the nanowire cross-section profile by laser irradiation at different incident angles. Metal-assisted chemical etching faithfully transferred the holes into silicon, yielding arrays of VA-SiNW with smooth walls and controlled lengths. This approach enables the fabrication of tailored ordered arrays of VA-SiNW with tunable diameters at desired locations on a same silicon wafer. Using sparse arrays of VA-SiNW as platforms for cell transfection, eGFP reporter gene was successfully delivered into HEK293 cells. The combination of near-field nanopatterning with metal-assisted chemical etching demonstrated here holds great promise for the fabrication of various functional surfaces.

Acknowledgements

We thank Prof. E. Arzt for his continuing support of the project and stimulating discussions. We also thank A. May and C. K. Akkan for their help in building the laser setup. Funding from the German Science Foundation (DFG) in the framework of Priority Programme 1420, from the Australia–Germany Researcher Mobility Programme and the DAAD-ATN travel grant scheme are gratefully acknowledged. This research was in part conducted and funded by the Australian Research Council Centre of Excellence in Convergent Bio-Nano Science and Technology (project number CE140100036). NHV was supported by an Alexander von Humboldt Foundation Fellowship.

References

[1] Cao A, Sudhölter E J R and C. P.M. de Smet L 2014 Silicon Nanowire Based Devices for Gas-Phase Sensing *Sensors* **14** 245-71

[2] Garnett E and Yang P 2010 Light Trapping in Silicon Nanowire Solar Cells *Nano Lett.* **10** 1082-7

[3] Kelzenberg M D, Boettcher S W, Petykiewicz J A, Turner-Evans D B, Putnam M C, Warren E L, Spurgeon J M, Briggs R M, Lewis N S and Atwater H A 2010 Enhanced absorption and carrier collection in Si wire arrays for photovoltaic applications *Nat. Mater.* **9** 239-44

[4] Zamfir M R, Nguyen H T, Moyen E, Lee Y H and Pribat D 2013 Silicon nanowires for Li-based battery anodes: a review *J. Mater. Chem. A* **1** 9566-86

[5] Alhmoud H Z, Guinan T M, Elnathan R, Kobus H and Voelcker N H 2014 Surface-assisted laser desorption/ionization mass spectrometry using ordered silicon nanopillar arrays *Analyst* **139** 5999-6009

[6] Shalek A K, Robinson J T, Karp E S, Lee J S, Ahn D-R, Yoon M-H, Sutton A, Jorgolli M, Gertner R S, Gujral T S, MacBeath G, Yang E G and Park H 2010 Vertical silicon nanowires as a universal platform for delivering biomolecules into living cells *PNAS* **107** 1870–5

[7] Elnathan R, Kwiat M, Patolsky F and Voelcker N H 2014 Engineering vertically aligned semiconductor nanowire arrays for applications in the life sciences *Nano Today* **9** 172

[8] Li Z, Song J, Mantini G, Lu M-Y, Fang H, Falconi C, Chen L-J and Wang Z L 2009 Quantifying the Traction Force of a Single Cell by Aligned Silicon Nanowire Array *Nano Lett.* **9** 3575-80

[9] Liu X and Wang S 2014 Three-dimensional nano-biointerface as a new platform for guiding cell fate *Chem. Soc. Rev.* **43** 2385-401

[10] Peng F, Su Y, Wei X, Lu Y, Zhou Y, Zhong Y, Lee S-T and He Y 2013 Silicon-Nanowire-Based Nanocarriers with Ultrahigh Drug-Loading Capacity for In Vitro and In Vivo Cancer Therapy *Angew. Chem. Int. Ed.* **52** 1457-61

[11] Michael T. Yang, Nathan J. Sniadecki and Chen C S 2007 Geometric Considerations of Micro- to Nanoscale Elastomeric Post Arrays to Study Cellular Traction Forces *Adv. Mater.* **19** 3119-23

[12] Choi W K, Liew T H and Dawood M K 2008 Synthesis of Silicon Nanowires and Nanofin Arrays Using Interference Lithography and Catalytic Etching *Nano Lett.* **8** 3799-802

[13] Mai T T, Lai C Q, Zheng H, Balasubramanian K, Leong K C, Lee P S, Lee C and Choi W K 2012 Dynamics of Wicking in Silicon Nanopillars Fabricated with Interference Lithography and Metal-Assisted Chemical Etching *Langmuir* **28** 11465−71

[14] Zhang P, Liu P, Siontas S, Zaslavsky A, Pacifici D, Ha J-Y, Krylyuk S and Davydov A V 2015 Dense nanoimprinted silicon nanowire arrays with passivated axial p-i-n junctions for photovoltaic applications *J. Appl. Phys.* **117** 125104

[15] Zhang J H, Li Y F, Zhang X M and Yang B 2010 Colloidal Self-Assembly Meets Nanofabrication: From Two-Dimensional Colloidal Crystals to Nanostructure Arrays *Adv. Mater.* **22** 4249-69

[16] Vogel N, Weiss C K and Landfester K 2012 From soft to hard: the generation of functional and complex colloidal monolayers for nanolithography *Soft Matter* **8** 4044-61

[17] Wu Y, Yan H and Yang P 2002 Semiconductor nanowire array: potential substrates for photocatalysis and photovoltaics *Top. Catal.* **19** 197-202

[18] Min W L, Jiang B and Jiang P 2008 Bioinspired Self-Cleaning Antireflection Coatings *Adv. Mater.* **20** 3914-8

[19] Li X 2012 Metal assisted chemical etching for high aspect ratio nanostructures: A review of characteristics and applications in photovoltaics *Curr. Opin. Solid State Mater. Sci.* **16** 71-81

[20] Han H, Huang Z and Lee W 2014 Metal-assisted chemical etching of silicon and nanotechnology applications *Nano Today* **9** 271-304

[21] Huang Z, Fang H and Zhu J 2007 Fabrication of Silicon Nanowire Arrays with Controlled Diameter, Length, and Density *Adv. Mater.* **19** 744-8

[22] Huang Z, Geyer N, Werner P, de Boor J and Gösele U 2011 Metal-Assisted Chemical Etching of Silicon: A Review *Adv. Mater.* **23** 285-308

[23] Huang S M, Sun Z, Luk'yanchuk B S, Hong M H and Shi L P 2005 Nanobump arrays fabricated by laser irradiation of polystyrene particle layers on silicon *Appl. Phys. Lett.* **86** 161911
[24] Piglmayer K, Denk R and Bäuerle D 2002 Laser-induced surface patterning by means of microspheres *Appl. Phys. Lett.* **80** 4693
[25] Brodoceanu D, Landström L and Bäuerle D 2007 Laser-induced nanopatterning of silicon with colloidal monolayers *Appl. Phys. A* **86** 313–4
[26] Zhou Y, Hong M H, Fuh J, Lu L, Luk'yanchuk B S, Wang Z B, Shi L P and Chong T C 2006 Direct femtosecond laser nanopatterning of glass substrate by particle-assisted near-field enhancement *Appl. Phys. Lett.* **88** 023110
[27] Born P, Blum S, Munoz A and Kraus T 2011 Role of the Meniscus Shape in Large-Area Convective Particle Assembly *Langmuir* **27** 8621-33
[28] Bauer C T, Wonn A, Brodoceanu D, Born P, Kroner E and Kraus T 2014 Size and shape evolution of PS particle layers during etching *Bioinspired, Biomimetic Nanobiomater.* **2** 130 –40
[29] Luk'yanchuk B S, Wang Z B, Song W D and Hong M H 2004 Particle on surface: 3D-effects in dry laser cleaning *Appl. Phys. A* **79** 747-51
[30] Rosenfeld A and Campbell E E B 1996 Picosecond UV-laser ablation of Au and Ni films *Appl. Surf. Sci.* **96** 439-42
[31] Huang S M, Wang Z A, Sun Z, Wang Z B and Luk'yanchuk B 2009 Theoretical and experimental investigation of the near field under ordered silica spheres on substrate *Appl Phys A* **96** 459-66
[32] Martín-Fabiani I, Siegel J, Riedel S, Boneberg J, Ezquerra T A and Nogales A 2013 Nanostructuring Thin Polymer Films with Optical Near Fields *ACS Appl Mater Interfaces* **5** 11402–8
[33] David C, Kühler P, Abajo F J G and Siegel J 2014 Near-field nanoimprinting using colloidal monolayers *Optics Express* **22** 8226-33
[34] Bäuerle D 2011 *Laser Processing and Chemistry* (Berlin: Springer)
[35] Hartmann J, Voigt P and Reichling M 1997 Measuring local thermal conductivity in polycrystalline diamond with a high resolution photothermal microscope *J. Appl. Phys.* **81** 2966-72
[36] Venkatakrishnan K, Tan B and Ngoi B K A 2002 Femtosecond pulsed laser ablation of thin gold film *Opt. Laser Technol.* **34** 199 - 202
[37] Burzo M G, Komarov P L and Raad P E 2003 Thermal Transport Properties of Gold-Covered thin films silicon dioxide *IEEE T. Compon. Pack. T.* **26** 80-8
[38] Thompson C V 2012 Solid-State Dewetting of Thin Films *Annu. Rev. Mater. Res.* **42** 399-434
[39] Ruffino F and Grimaldi M G 2015 Controlled dewetting as fabrication and patterning strategy for metal nanostructures *Phys. Status Solidi A* **212** 1662 -84
[40] Kallepalli L N D, Grojo D, Charmasson L, Delaporte P, Uteza O, Merlen A, Sangar A and Torchio P 2013 Long range nanostructuring of silicon surfaces by photonic nanojets from microsphere Langmuir films *J. Phys. D: Appl. Phys.* **46** 145102
[41] Guo W, Wang Z B, Li L, Whitehead D J, Luk'yanchuk B S and Liu Z 2007 Near-field laser parallel nanofabrication of arbitrary-shaped patterns *Appl. Phys. Lett.* **90** 243101
[42] Bonde S, Buch-Månson N, Rostgaard K R, Andersen T K, Berthing T and Martinez K L 2014 Exploring arrays of vertical one-dimensional nanostructures for cellular investigations *Nanotechnology* **25** 362001
[43] Kim W, Ng J K, Kunitake M E, Conklin B R and Yang P 2007 Interfacing Silicon Nanowires with Mammalian Cells *J. Am. Chem. Soc.* **129** 7228 - 9